accepted in Construction and Building Materials, June 2021

1

Advancement in measuring the hydraulic conductivity of porous asphalt pavements

F. Giuliani[a], D. Petrolo[a], L. Chiapponi[1a], A. Zanini[a], S. Longo[a]

[a] *Department of Engineering and Architecture, University of Parma, Parco Area delle Scienze 181/A, 43124 Parma, Italy*

Abstract

The measurement of the in situ hydraulic conductivity of porous asphalt pavements, K, is a matter of practical interest; however, there are cases where current techniques are difficult to use. Several methods are documented in literature, mainly based on permeameters with water as fluid. Using water has its advantages, as it is straightforwardly related to the drainage problem during rain storms, but it also involves some major issues, especially on field studies. For instance, the time necessary to reach the steady state is too long and the necessary amount of water could not be available. In addition, non-repeatability and hysteresis phenomena can occur, also due to air bubbles confined in the porous matrix. In the present paper, we describe a novel test method for measuring K using air at low pressure as fluid. The proposed permameter was first tested in the laboratory, in order to (i) validate the theoretical relationships between $K_{\mathrm{H_2O}}$ and K_{air}, and (ii) define a model to evaluate an equivalent length scale for asphalt pavements, L_{eq}, as a function of the thickness of the porous layer (this is useful when one-dimensional formulations are adopted in the case of three-dimensional plates or in-situ measurements). Finally, the protocol and methodology were validated on two sites in Italy (Monza, Milan, and Poviglio, Reggio Emilia) where K_{air} was measured by the air field permeameter, and compared with $K_{\mathrm{H_2O}}$, measured by a standard falling head permeameter. The technique allows the determination of the hydraulic conductivity on the basis of the ratio between pressure difference and flow rate, and of L_{eq}.

Keywords: Porous asphalt pavements, pollution management, hydraulic conductivity, permeameters

1. Introduction

Road safety during rainfall events is a major concern and has pushed the development of porous pavements able to drain most of the water and guarantee an adequate wet grip. The pervious materials, not only allow storm water to infiltrate and flow over an impervious surface beneath, but also filter pollutants. In urban areas, these materials

[1] Corresponding author: luca.chiapponi@unipr.it

help managing run-off, reducing the peak discharge in the surface water bodies, as well as reducing noise [1, 2, 3, 4]. On the downside, clogging effects happen: sediments and tyre rubber particles transported by runoff tend to deposit and block the interconnected pores, reducing the hydraulic conductivity [5, 6, 7]. In addition, the sound absorption by the pavement may be reduced up to a factor of 25% [8]. A second relevant disadvantage is the formation of ice on motorways and roads in cold regions. To prevent this, salts or various organic compounds, which lower the freezing point of water, are spread, despite the non ecological consequences to the natural environment [9, 10, 11, 12]. To limit environmental pollution, fluids with programmed rheological behaviour, able to penetrate into the pores of draining road surfaces, can be used to reduce the hydraulic conductivity (and therefore the dispersion) of brines and/or organic mixtures used for anti-icing and de-icing.

Since the hydraulic conductivity is a fundamental parameter for a proper functioning of porous asphalt pavements, and tends to be altered by the aforementioned phenomena, its value must be checked during construction and maintenance. An accurate and low cost procedure for measuring the hydraulic conductivity is then required, with a simple and reliable use for in situ measurements.

Several methods have been proposed in literature to evaluate the hydraulic conductivity of asphalt concrete and pavements, but only a few of them aim at measuring the hydraulic conductivity in situ. Water is the most frequently adopted fluid, because it is straightforwardly related to the drainage problem on roads and highways during rain storms.

Some standardised water permeameters are listed below.

The European Standard EN 12697-40:2005(E) [13] describes a method to determine the in situ relative hydraulic conductivity of porous pavements by means of a water permeameter. The methodology is low cost, easy to use and it ensures the repeatability of the measurements.

Other two largely used devices are the National Center for Asphalt Technology (NCAT) falling head permeameter and the constant head permeameters based on the American Society for Testing and Materials (ASTM) C1701/C1701M [14] and ASTM C1781/C1781M [15] methods. Even if both methods can effectively be used with all pavement types, the hydraulic conductivity values measured with the NCAT method can be $1 - 9$ times higher than those measured with the ASTM method [16, 17].

A low cost falling head permeameter, the Laboratorio Caminos Santander (LCS) device, was also built by [6] according to the Spanish standard NLT 327/00 [18]. They modelled the hydraulic conductivity of their specimens with the Horton equations, with a satisfactory comparison with the in situ measurements.

Nevertheless, water is not the most convenient fluid to use when we are interested in measuring the hydraulic conductivity of porous asphalt pavements. The main reason is that the porous media of interest are generally not fully saturated and the analysis of the data requires a mathematical formulation with further complexities [see, e.g. 19]. In addition, the porous media should be saturated at the bottom, and tests should be performed in steady state conditions. This is not easily achievable in situ.

A more convenient way to evaluate the hydraulic conductivity is to use air as fluid instead of water. The main advantages are that (i) a little time is necessary to establish pressure flow equilibrium; (ii) tests can be repeated without the influence of residual water in the porous medium and without the disturbances due to air trapped in the meati; (iii) the nature of the test is non destructive, as the crack sizes are not affected by

gas flows, if applied for short period and with a low average pressure, [20]. As a matter of fact, some physical phenomena induced by water may alter the hydraulic conductivity of pavements (e.g., the crack propagation and the effect of surface tension in unsaturated media). It is difficult to reproduce such effects at a laboratory scale or during field studies using water as a fluid, so air guarantee more reliable values of the conductivity of the undisturbed medium [21, 22].

A long list of experiments on conductivity measurements with the use of air is available for a wide variety of porous media [23, 24, 25, 26, 27, 28, 22, 29]. Further details can be found in Varganega (2012) [30], where an extensive literature review on the conductivity of asphalt concrete is presented. The author pointed out that field conductivity measurements do not match well with laboratory measurements, although there is some correlation. He took into consideration and described all the possible influencing factors, as the air voids, the air voids connectivity, the mix gradation, the mixture binder content, the nominal maximum aggregate size and the lift thickness. Another possible explanation of the discrepancies is the possible anisotropy of the porous structure in asphalt concrete. Both laboratory experiments [31] and computational simulations [32, 33] show that the conductivity in the horizontal direction is greater than the vertical.

Most of the literature methods are based on an integral approach and they do not go into diriment fluid mechanics details. For instance, we remind the readers that Darcy law is strictly valid in laminar regime, for Reynolds number $\mathrm{Re} \leq 10$, and that it is replaced by other approximations for larger values of Re. In addition, non linear relation between gradient pressure and flow rate is often attributed to turbulence. As a matter of fact, turbulence is not triggered at the microscale of the voids of a porous medium. It is the sequence of contractions and expansions encountered by the fluid advancing in the porous matrix, or in the fissured medium, which induces Borda-Carnot losses.

A more detailed analysis is impeded by the evidence that many of the variables and parameters, such as path length and tortuosity, are known with limited accuracy. A relevant issue is the rheology of the fluid, which is Newtonian in most cases, but shows non-Newtonian behavior in some special cases. The slurry flowing on the asphalt pavement and infiltrating in the initial phase of heavy rainstorms after a long period of drought, with suspended particles and high concentration of pollutants, is prone to behave like an Ostwald-deWaele or Herschel-Bulkley fluid. This adds up further complexities, although several theoretical models of non-Newtonian fluids flowing in porous media [34, 35] and in fractures and fissures [36, 37] have been experimental validated. These aspects are left for future analysis with a perspective of improving the interpretation of hydraulic conductivity data for a better road and highway maintenance plan.

The main objective of this paper is to describe a very easy and immediate way to measure the in situ permeability of porous asphalt pavements, using air as fluid. We derive a very simple theoretical model based on the physics of the drainage process, to calculate an equivalent conductivity length scale, L_{eq}, as a function of the only thickness of the porous asphalt layer. In situ, the only measurement of the ratio between pressure and inflow rate is required to evaluate the air conductivity of the asphalt pavements, together with the estimate of L_{eq}. Then, the water conductivity can be estimated on the basis of dimensional analysis.

First of all, to reach this goal, some cylindrical specimens made of glass beads were tested as a benchmark. The experimental value of the air conductivity, K_{air}, was compared with the water conductivity, $K_{\mathrm{H_2O}}$, also obtained by empirical formulas found in

literature. So, the conductivity ratio between the two fluids was found. In a second step, the air conductivity was measured both on asphalt plates and on cylindrical samples. Results were used to derive an equivalent length scale, L_{eq}, as a function of the thickness of the asphalt plate h. Finally, a series of field tests were conducted to compare the in situ air conductivity of a porous asphalt pavement with the water conductivity measured by a falling head permeameter. The experimental values of the ratio between conductivity to water and to air were also compared to the theoretical values predicted by dimensional analysis.

The paper is structured as follows. The theoretical approach to the problem is discussed in terms of dimensional analysis in § 2. The experimental setup and protocol are presented in § 3, while the results of laboratory tests and field cases are detailed in § 5. The conclusions are given in § 6.

2. Hints from dimensional analysis

Dimensional analysis can be used for a conceptual schematic of the fluid filtration processes in porous media and fractures and to retrieve similarity laws, see e.g. [38, 39] for details on the principles and applications. Filtration depends on geometrical variables related to the characteristics of the porous medium, like the diameter of the meati, D, the characteristic length path, L, and the porosity, n, and on the physical parameters of the fluid like the density, ρ, the dynamic viscosity μ, and the velocity, u. Other physical quantities which influence the filtration processes are the acceleration due to gravity, g, and the total head, H, better considered as head variation ΔH. In the presence of gas, also a slip between the gas molecules and solid walls occur, the so called Klinkenberg effect [40], with an increase of conductivity depending on the mean free path of molecules, l_m. In the most general case, we can describe the filtration process as a function of these variables and parameters:

$$f\left(\Delta H, L, \rho, g, D, u, \mu, n, l_m\right) = 0, \tag{1}$$

where n is already dimensionless. The rank of the dimensional matrix in a system of class M, L, T is three, hence relying on Buckingham's theorem we can express the process as a function of five dimensionless groups plus the porosity. Selecting a basis, e.g. D, ρ, g, a set of independent variables in a system of class M, L, T, the function of the possible dimensionless groups is

$$f'\left(\frac{\Delta H}{D}, \frac{L}{D}, \frac{u^2}{gD}, \frac{\rho D u}{\mu}, n, \frac{l_m}{D}\right) = 0, \tag{2}$$

where $u^2/gD \equiv \mathrm{Fr}$ is the Froude number, $\rho D u/\mu \equiv \mathrm{Re}$ is the Reynolds number, $l_m/D \equiv \mathrm{Kn}$ is the Knudsen number. Experimental evidences indicate that a more suitable dimensionless group is the energy dissipation rate, $J = -\Delta H/L$, obtained as a combination of $\Delta H/D$ and L/D, and that L/D is not relevant if it is very large, in the limit $L/D \to \infty$. Therefore, by expressing the J governed variable as a function of the governing variables, we can write:

$$J = \tilde{f}\left(\mathrm{Fr}, \mathrm{Re}, n, \mathrm{Kn}\right). \tag{3}$$

The Knudsen number for a gas can be computed adopting the expression of the mean free path of molecules as a function of the temperature θ, of pressure p, of the diameter of the pores and of the Boltzmann's constant $\kappa = 1.38 \cdot 10^{-23}\ \mathrm{J\,K^{-1}}$

$$l_m = \frac{\kappa}{\pi\sqrt{2}D^2}\frac{\theta}{p}, \tag{4}$$

hence

$$\mathrm{Kn} = \frac{l_m}{D} \equiv \frac{\kappa}{\pi\sqrt{2}D^3}\frac{\theta}{p}. \tag{5}$$

Klinkenberg suggested that the gas intrinsic permeability varies as

$$k = k_\infty \left(1 + 8\,c\,\mathrm{Kn}\right), \tag{6}$$

where k_∞ is the asymptotic intrinsic permeability for $p \to \infty$ (or very large D) and c is an experimental coefficient slightly less than unity. A more common expression for the intrinsic permeability for gases is

$$k = k_\infty \left(1 + \frac{b}{p}\right), \tag{7}$$

where

$$b = 8\,c\,\frac{\kappa\theta}{\pi\sqrt{2}D^3} \tag{8}$$

is the Klinkenberg slip coefficient. In brief, increasing pressure/diameter reduces the Knudsen number and the intrinsic permeability. It is noteworthy that Klinkenberg effect is relevant only for low permeability media [41, found that the ratio between permeability to argon and to water is of $\mathcal{O}(10)$ for clay rich rocks], with typical values $b = 10^3 - 10^5$ Pa for $k = 10^{-12} - 10^{-18}$ m^2 [42], and is irrelevant for porous asphalt pavements with $D = \mathcal{O}(10^{-3}$ m) even at an average ambient pressure, with Kn $\to 0$. As a general consideration, we add that the formulation of Klinkenberg effect in terms of variation of the intrinsic permeability (a geometric property) is odd: the effect of the slip is on the flow, and should be better described in terms of variation of the conductivity.

On the basis of experimental evidence, eq.(3) is rearranged as:

$$\frac{\gamma J D}{\rho u^2} = \frac{\Phi(n)}{\mathrm{Re}}, \tag{9}$$

where $\Phi(n)$ is a function that depends on n. If we isolate u, we get:

$$u = \frac{1}{\Phi(n)}\frac{\gamma D^2}{\mu}J = KJ, \tag{10}$$

where K represents the conductivity. Equation (10) is the classical Darcy equation, valid for small Re and also valid for gases if Kn $\to 0$.

The similarity condition requires the equality of Re and Fr and n in the two similar processes, so we can write:

$$\begin{cases} \dfrac{r_\gamma r_J \lambda}{r_\rho r_u^2} = 1, \\ \\ \dfrac{r_\rho r_u \lambda}{r_\mu} = 1, \\ \\ r_n = 1. \end{cases} \tag{11}$$

where r_i is the scale ratio for the quantity i, and λ is the length scale. We are interested in measuring the conductivity of a porous medium to air instead of water, for the case $\lambda = 1$. The scale ratios r_ρ and r_μ are known parameters, so we can compute:

$$\begin{cases} r_J = r_u^2, \\ \\ r_u = \dfrac{r_\mu}{r_\rho}. \end{cases} \tag{12}$$

The ratio r_μ / r_ρ represents the scale ratio for the kinematic viscosity r_ν, so $r_\mu / r_\rho = \nu_{\mathrm{H_20}} / \nu_{\mathrm{air}} \approx 10^{-1}$. Hence,

$$\begin{aligned} \frac{J_{\mathrm{H_20}}}{J_{\mathrm{air}}} \approx 10^{-2} &\longrightarrow J_{\mathrm{H_20}} \approx 10^{-2} J_{\mathrm{air}} \\ \frac{u_{\mathrm{H_20}}}{u_{\mathrm{air}}} \approx 10^{-1} &\longrightarrow u_{\mathrm{H_20}} \approx 10^{-1} u_{\mathrm{air}}. \end{aligned} \tag{13}$$

If the length path is the same, since we are dealing with the same porous medium with the same geometry, we can also write

$$\Delta p_{\mathrm{H_20}} \approx 10^{-2} \, \frac{\gamma_{\mathrm{H_20}}}{\gamma_{\mathrm{air}}} \, \Delta p_{\mathrm{air}} \approx 10 \, \Delta p_{\mathrm{air}}. \tag{14}$$

This means that at fixed Re and fixed Fr, the water pressure difference must be ten times greater than the air, and the water velocity is ten times lower than air. Also $Q_{\mathrm{H_20}} \approx 0.10 \, Q_{\mathrm{air}}$, since the cross-section area depends on $\lambda = 1$.

Finally, if we evaluate the scale ratio for the conductivity, using eq.(10), we obtain

$$r_K = \frac{K_{\mathrm{H_20}}}{K_{\mathrm{air}}} = 10 \quad \longrightarrow \quad K_{\mathrm{H_20}} \approx 10 \, K_{\mathrm{air}}. \tag{15}$$

3. Experimental set-up

The laboratory tests were carried out in the Laboratory of Hydraulics of the University of Parma, the field tests were performed in Monza (Milan, Italy) and Poviglio (Reggio Emilia, Italy). Three different permeameters were adopted, briefly described in the following.

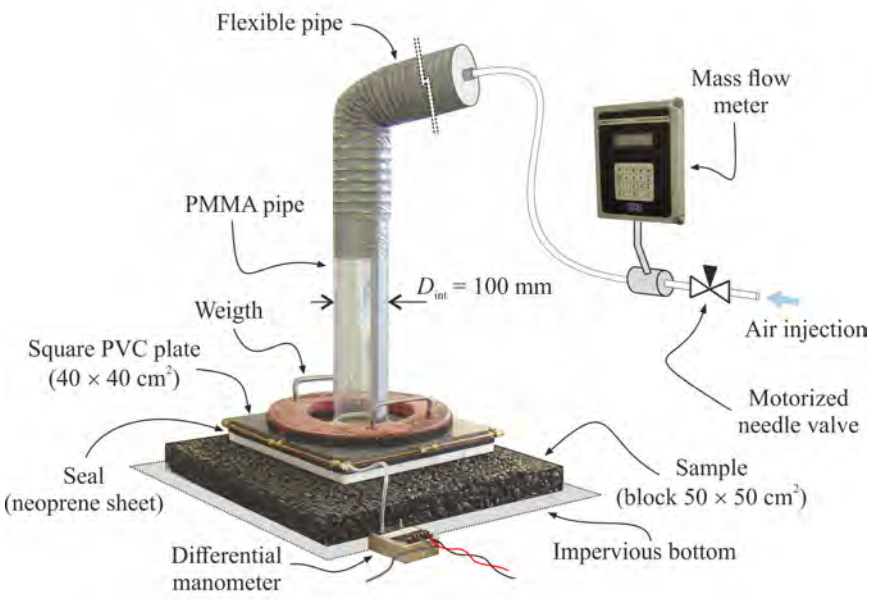

Figure 1: Experimental setup: the field permeameter.

3.1. Air field permeameter

Our experimental device is similar to the field permeameter used by [43], with a pipe of Polymethylmethacrilate (PMMA) with internal diameter $D_{\text{int}} = 100\,\text{mm}$. The lower end of the pipe is joined to a square plastic plate (polyvinyl chloride, PVC) $40 \times 40\,\text{cm}^2$ and 2 cm thick, which must be placed on the asphalt plate, while the other end is connected to the air supply line. A neoprene sheet is placed between the PVC and the asphalt plates, and also vacuum grease is applied on the seal surfaces to avoid air leakage. The pipe is long enough to allow the air jet exiting from a 8 mm tube to expand and the flow to reach homogeneity before infiltrating in the porous medium. A circular crown-shaped iron weight guarantees uniform and reproducible force on the square plate in contact with the porous asphalt plate. The air flow rate is controlled by a motorized needle valve, and is measured by a thermal mass flow meter (Kurz model 502-6A), with a range $0 - 1.00\,\text{l}\,\text{s}^{-1}$ and with an accuracy of 2% FS. The differential pressure is measured through a capacitive differential manometer (Ashcroft XLDP), with an accuracy of 0.5% FS in a range $0 - 65.0$ Pa. Before each test, the differential manometer was calibrated with a calibrator Druck 601-F. The active port of the manometer is connected to the PVC plate with several radial pipes, in order to average the pressure fluctuations, the other port is connected to the atmospheric ambient. An electric valve also allows the periodic connection of the active port to the atmospheric pressure, in order to correct any bias. The experimental apparatus is shown in figure 1.

The instruments and the valves are controlled through a DAQ system with a data rate of 20 Hz. All the tests are executed by progressively opening the needle valve and acquiring the differential pressure and the air flow rate, and then progressively closing the valve, up to the closure. This cycle is repeated twice.

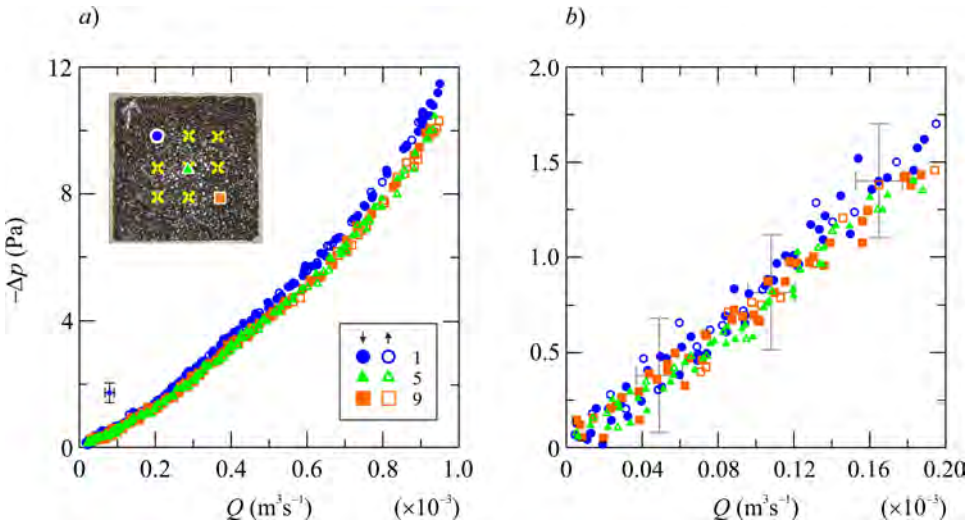

Figure 2: Pressure-discharge measurements for the 30 mm thick plate. *a*) Results for measurements with the permeameter centered in three different points shown in the inset; *b*) pressure-discharge measurements for the same experiment in *a*), in the limit $Q < 0.20 \cdot 10^{-3}$ m^3 s^{-1}. Empty and filled symbols refer to the increasing and decreasing flow branch, respectively. Only one point in two hundreds is shown for clarity, with error bars equal to the instrumental accuracy.

Figure 2a shows the first cycle of increasing-decreasing air flow rate for the same plate (thickness $h = 30$ mm) in three of the nine measurement points. Notice that it is possible to center the permeameter in any position of the sample (ensuring a minimum distance from the boundary), in order to estimate a possible non homogeneous behavior of the asphalt plate. The selected measurement points are marked in figure 2a by different symbols and they are set 10 cm apart from one another, in both directions. The measurement data show no hysteresis, with overlap of the branches of increasing and decreasing air flow rate, and with a modest difference amongst the three sets of measurements. The relationship flow rate–differential pressure is non-linear, as a consequence of the Reynolds number which progressively increases beyond the limit of Darcy flow regime. However, for $Q < 0.20 \cdot 10^{-3}$ m^3 s^{-1} a linear trend is observed, as shown in figure 2b, with a relationship:

$$-\Delta p = aQ, \tag{16}$$

where a is the slope of the interpolating straight line.

The Darcy law (10) can be written as:

$$K = \frac{u}{J} = -\frac{QL\gamma_{\text{air}}}{A\Delta p}, \tag{17}$$

where the velocity u is the ratio between the flow rate, Q and the cross-section area A, the average energy gradient, $J = -\Delta H/L$, is the change in the head ΔH, over the length path, L. If the fluid is air, one can write $\Delta H = \Delta p/\gamma_{\text{air}}$, with γ_{air} equal to 12.02 N m^{-3}. Using eq.(16), eq.(17) becomes:

$$K = \frac{L\gamma_{\text{air}}}{Aa}. \tag{18}$$

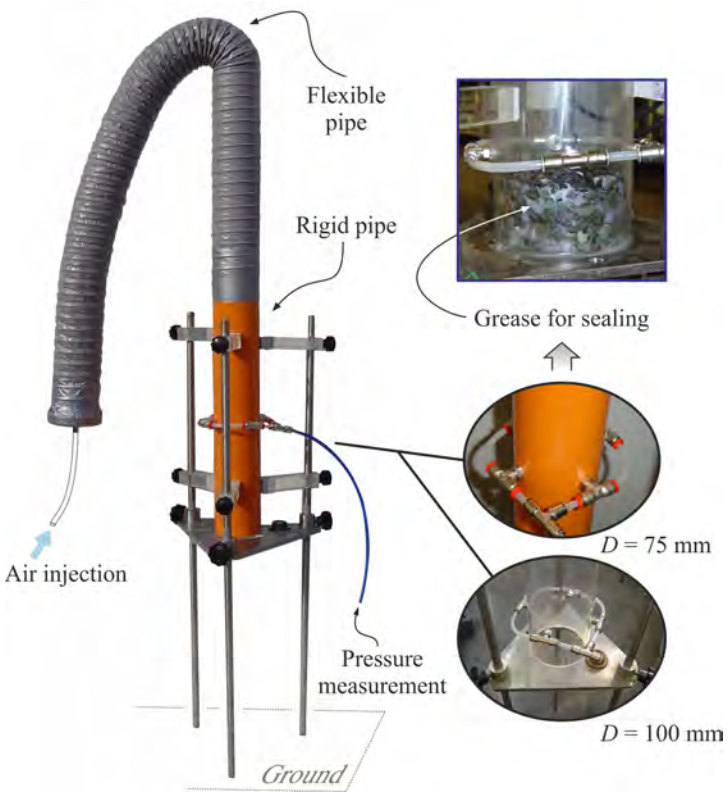

Figure 3: Experimental setup: 1-D permeameter.

3.2. 1-D air laboratory permeameter

In addition to the permeameter described in § 3.1, the permeameter shown in figure 3 has been constructed in order to estimate the one-dimensional (1-D) conductivity of the asphalt sample.

The 1-D permeameter consists of a rigid pipe with diameter equal to 75 mm or 100 mm (two versions with different diameter, D were realized). The lower end of the pipe is designed to laterally confine a cylindrical sample extracted from the asphalt plates, and the sealing between the sample and the inner surface of the pipe is secured by the application of vacuum grease. The other end of the pipe is connected to the air supply circuit. The experimental procedure and all the instruments are the same as described for the field permeameter in §3.1, with the only difference that the active port of the manometer is directly connected to the pipe by means of four radial intakes located in a section a few centimetres above the sample.

3.3. Water falling head permeameter

A third permeameter was used to measure the hydraulic conductivity in situ. The falling head permeameter used for this purpose is shown in figure 4. This permeameter

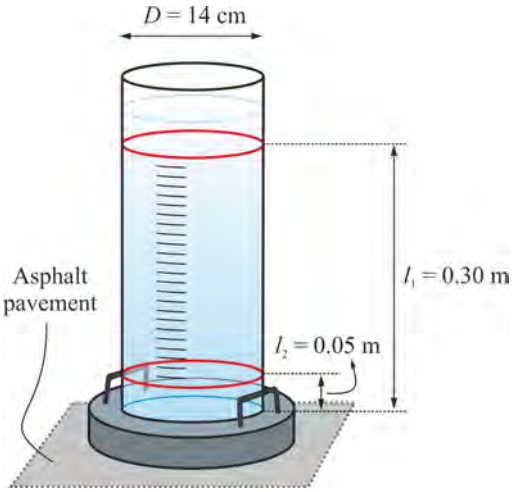

Figure 4: Falling head permeameter.

has a diameter of 14 cm and a total height of 35 cm. The hydraulic conductivity can be computed as

$$K_{\mathrm{H_2O}} = \frac{Ah}{A'\,\Delta t} \ln\left(\frac{l_1}{l_2}\right) \tag{19}$$

where A is the cross-section area of the standpipe, h is the thickness of the asphalt plate, A' is the sample cross-section, here equal to $A' = A$, and Δt is the recorded time interval for the water column to flow though the sample, from the initial level $l_1 = 0.30$ m to the final level $l_2 = 0.05$ m.

4. Materials and methods

4.1. Glass beads specimens

Some specimens with different mixtures of glass beads with diameter $d = 1, 2, 3$ mm were tested with the 1-D permeameter with air, for an estimate of the scale factor $r_K = K_{\mathrm{H_2O}}/K_{\mathrm{air}}$. We prepared (i) homogeneous specimens, using uniformly sized beads; (ii) stratified specimens, with three homogeneous horizontal layers of beads with increasing diameter from top to bottom ($1 - 2 - 3$ mm) and vice-versa ($3 - 2 - 1$ mm); (iii) heterogeneous mixtures by randomly mixing the beads of $1, 2, 3$ mm, or $2, 3$ mm, or $1, 3$ mm. All the specimens have a diameter of 90 mm and height of 60 mm. The porosity of approximately $n \approx 37\%$ and the void ratio $e = n/(1 - n) \approx 60\%$ were measured as described by [44]. The specimens were placed inside a special holder with a grid at the base that could hold the beads and support the weight of the specimen, without interfering with the air flow. An O-ring seal was inserted between the holder and the inner radius of the permeameter in order to prevent any air leakage.

A limited number of specimens (tests $3-4-5-9-10$ of table 1) were also tested with a standard 1-D permeameter (Matest S245-01) with water. This device is commonly used to determine the permeability of granular, gravel and sand soils. The specimen is formed

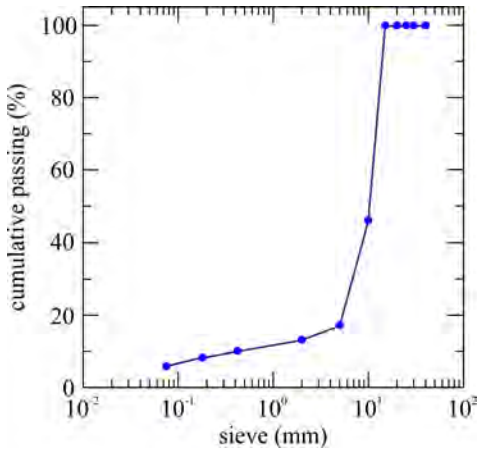

Figure 5: Aggregate grading curve of the porous asphalt square plates.

in an acrylic permeability cell, and water is passed through it from a constant level tank. The permeability cell has pressure points at different levels which are connected to the manometer tubes fixed on a stand with graduated scale.

4.2. Porous asphalt square plates and cylindrical samples

In order to reproduce common draining asphalt plates, we built porous asphalt square plates, 50×50 cm^2, with variable thickness, with a discontinuous aggregate grading curve, a polymer modified asphalt content of 4.2% by weight of aggregate, and a void ratio of 17%. The aggregate grading curve is shown in figure 5. The polymer modified asphalt was produced by ENI Company and has the following characteristics: PMA 50/70-93.5, penetration at 25°C = 5.5 mm according to UNI EN 1426:2015 (included into "Specifications for paving grade bitumens" EN 12591:2009). The binder performance grade is PG 82-22 according to AASHTO M-320 Edition 2017. The glass fiber content is 0.3% by weight of the aggregate.

The density of the samples was approximately 2000 kg m^{-3}. The samples were prepared by (i) heating up the mixture in a furnace at 180 °C for 6-8 hours; (ii) spreading the mixture in a metallic framework; (iii) pressing it with a mechanical press which simulates the action of road rollers and homogenizes the thickness of the plate; (iv) further compacting the mixture with a mechanical arm handling a cylindrical sector that reproduces the field compaction, as shown in figure 6a. The thickness of the plates were set at $h = 30, 45, 65, 70$ and 105 mm. As in real road pavements, where an impervious interface, made of a hot bituminous emulsion, is usually present beneath the porous near surface layers, we positioned the asphalt plates on an impervious surface, but made of wood. A typical example of asphalt plate is shown in figure 6c.

After the square plates were tested with the field permeameter, they were cored for measuring the vertical 1-D conductivity by means of a core drill, as illustrated in figure 6b.

In order to guarantee a sufficient lateral confinement, we decided to extract cylindrical samples with a diameter of 75 mm vertically from the central area of each plate.

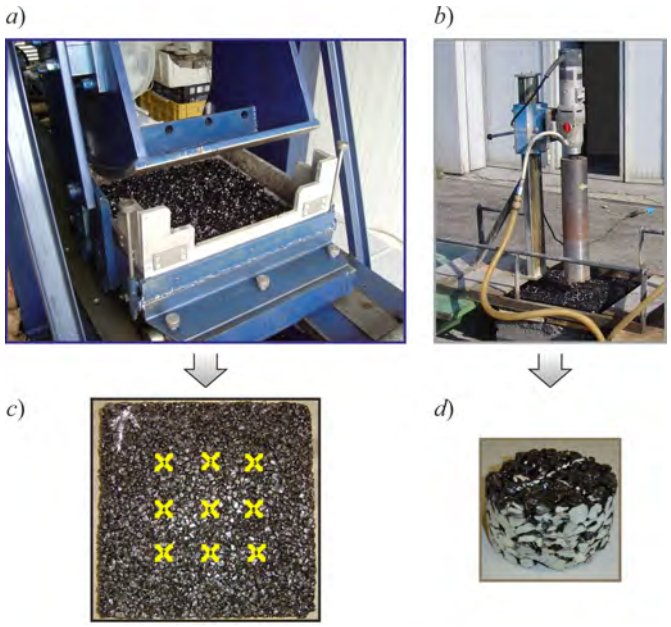

Figure 6: Preparation of the plates and samples. *a*) Laboratory machine used to create asphalt plates with variable thickness and 50×50 cm^2; *b*) driller coring the asphalt plates; *c*) asphalt plate ready to be tested with nine markers for the K_{air} measurements and an arrow indicating the top surface of the plate; *d*) sample cored from the plate, to be tested with 1-D permeameter.

Unfortunately, all the samples cored from the 30 mm thick plate crumbled, while only one sample from the 45 mm thick plate survived. From the 65 mm thick plate we cored three samples with a diameter of 75 mm and five samples with a diameter of 100 mm in order to compare different geometries. From the 105 mm thick plate we extracted two cores, with height of 65 mm. A typical example of cylindrical sample is shown in figure 6d. We also attempted to core samples in the horizontal direction in order to study possible anisotropy effects, but due to the limited thickness of the plates it was not possible to guarantee the necessary lateral confinement.

4.3. Experimental plan

Table 1 lists all the experiments in the laboratory.

Two further series of field tests were run in two available field sites. For some of the field tests, the results for the air conductivity, K_{air}, were compared with the water conductivity, $K_{\text{H}_2\text{O}}$ measured by the falling head permeameter. The data collected on a service road inside the Monza (Milan, Italy) racetrack are listed in table 2, where Δt_1, Δt_2, Δt_3 are three measurements with the falling head permeameter and $\overline{\Delta t}$ is the mean value. The data collected on a urban road under construction in Poviglio (Reggio Emilia, Italy) are listed in table 3.

test #	Permeameter	Medium	d (mm)	h (mm)	D (mm)	a ($\mathrm{Pa\,m^{-3}\,s}$) ($\times 10^5$)	K_{air} ($\mathrm{m\,s^{-1}}$) ($\times 10^{-3}$)	$K_{\mathrm{H_2O}}$ ($\mathrm{m\,s^{-1}}$) ($\times 10^{-3}$)
1	1D	GBh	0.5	60	90	3.422	0.40	
2	1D	GBh	0.75	60	90	3.074	0.44	
3	1D	GBh	1	60	90	1.805	0.64	10.59
4	1D	GBh	2	60	90	0.599	1.85	30.68
5	1D	GBh	3	60	90	0.316	3.87	56.3
6	1D	GBs	1-2-3	60	90	0.929	1.22	
7	1D	GBs	3-2-1	60	90	0.974	1.16	
8	1D	GBm	1,2,3	60	90	1.123	1.01	
9	1D	GBm	1,3	60	90	1.584	0.72	11.24
10	1D	GBm	2,3	60	90	0.439	2.58	31.91
11	1D	A	-	45	75	0.151	8.11	
12	1D	A	-	65	75	0.282	6.27	
13	1D	A	-	65	100	0.130	7.68	
14	1D	A	-	65	75	0.301	5.88	
15	F	A	-	30	100	0.064	6.79	
16	F	A	-	45	100	0.044	7.56	
17	F	A	-	65	100	0.048	5.69	
18	F	A	-	70	100	0.038	6.92	
19	F	A	-	105	100	0.030	7.44	

Table 1: List and parameters of the laboratory experiments. "F" stands for field permeameter (used in the laboratory with square asphalt plates) and "1D" for the 1-D permeameter. The medium is indicated by the following abbreviations: "A" stands for asphalt plate and "GB" for glass beads. In the case of experiments performed with glass beads of different size, GBh stands for homogeneous specimens, GBs for stratified specimens while GBm for an heterogeneous mixtures. d is the diameter of the glass beads, h is the thickness of the plate, D is the internal diameter of the permeameter, a is the inclination of the straight line fitting the $(-\Delta p, Q)$ data, K_{air} is the air conductivity and $K_{\mathrm{H_2O}}$ is the water conductivity.

test #	a ($\mathrm{Pa\,m^{-3}\,s}$) ($\times 10^5$)	K_{air} ($\mathrm{m\,s^{-1}}$) ($\times 10^{-3}$)	Δt_1 (s)	Δt_2 (s)	Δt_3 (s)	$\overline{\Delta t}$ (s)	$K_{\mathrm{H_2O}}$ ($\mathrm{m\,s^{-1}}$) ($\times 10^{-3}$)
M1	0.909	0.28	41	47	-	44	2.9
M2	0.735	0.35	-	-	-	-	-
M3	0.881	0.29	-	-	-	-	-
M4	0.686	0.38	34	38	-	36	3.5
M5	0.647	0.40	-	-	-	-	-
M6	0.599	0.43	-	-	-	-	-
M7	0.589	0.44	-	-	-	-	-
M8	0.545	0.47	28	31	33	31	4.1
M9	0.476	0.54	-	-	-	-	-
M10	0.444	0.58	-	-	-	-	-
M11	0.449	0.57	-	-	-	-	-
M12	0.570	0.45	22	23	-	23	5.6
M13	0.617	0.42	-	-	-	-	-
M14	0.621	0.41	-	-	-	-	-
M15	0.633	0.41	27	28	29	28	4.5
M16	0.605	0.43	-	-	-	-	-
M17	0.566	0.46	-	-	-	-	-

Table 2: List of the field tests performed in Monza on a porous asphalt pavement with thickness $h = 70$ mm. K_{air} was estimated with the field permeameter, $K_{\mathrm{H_2O}}$ with the falling head permeameter.

test #	a ($\mathrm{Pa\,m^{-3}\,s}$) ($\times 10^5$)	K_{air} ($\mathrm{m\,s^{-1}}$) ($\times 10^{-3}$)	Δt (s)	$K_{\mathrm{H_2O}}$ ($\mathrm{m\,s^{-1}}$) ($\times 10^{-3}$)
P1	0.350	1.01	-	-
P2	0.247	1.43	16.65	4.3
P3	0.307	1.15	-	-
P4	0.446	0.79	-	-
P5	0.301	1.17	12.15	5.9
P6	0.524	0.67	-	-
P7	0.448	0.79	-	-
P8	0.404	0.88	14.25	5.0
P9	0.441	0.80	-	-
P10	0.283	1.25	-	-

Table 3: List of the field tests performed in Poviglio on a porous asphalt pavement with thickness $h = 40$ mm. K_{air} was estimated with the field permeameter, $K_{\mathrm{H_2O}}$ with the falling head permeameter.

5. Results

5.1. Validation of the theoretical model

To prove that the conductivity scale ratio $r_K = \mathcal{O}(10)$, as predicted by dimensional analysis in §2, we performed tests $1-7$ listed in table 4. The experimental values of the air conductivity, K_{air}, were computed according to eq.(18), considering a length path equal to the height of the sample, $h = 65$ mm, the cross-section area A of the permeameter, and the parameter a.

On the other side, the value of the hydraulic conductivity for water, $K_{\text{H}_2\text{O}}$, was calculated following different approaches [45].

Terzaghi (1925) [46] proposed that the hydraulic conductivity should be computed as

$$K_{\text{H}_2\text{O}} = \frac{g}{\nu} C_T \left(\frac{n - 0.13}{\sqrt[3]{1-n}} \right)^2 d_{10}^2, \tag{20}$$

where $C_T = 10.7 \cdot 10^{-3}$ for smooth grains, while according to [47]:

$$K_{\text{H}_2\text{O}} = \frac{g}{\nu} C_Z \left(\frac{n}{1-n} \right)^2 d_e^2, \tag{21}$$

where $C_Z = 2.4 \cdot 10^{-3}$ for uniform sand with smooth and rounded grains. Sauerbrey (1932) [48] proposed that:

$$K_{\text{H}_2\text{O}} = \frac{g}{\nu} C_S \frac{n^3}{(1-n)^2} d_{17}^2 \tag{22}$$

for soils with an effective diameter up to 5 mm, with $C_S = 3.75 \cdot 10^{-3}$. The equation derived by Kozeny-Carman [49] can be used for silts, gravel and gravel sands:

$$K_{\text{H}_2\text{O}} = \frac{g}{\nu} \frac{1}{C_{KC}} \frac{1}{S_0^2} \frac{n^3}{(1-n)^2}, \tag{23}$$

where S_0 is the specific surface of particles, equal to $S_0 = 6/d$ for uniform spheres and $C_{KC} = 4.8$. Moreover, the approach by [50] suggests that:

$$K_{\text{H}_2\text{O}} = 5.39 \cdot 10^4 \frac{D^2 e^3}{(1+e)}, \tag{24}$$

where D is the diameter of the particles, e is the void ratio. Equation (24) refers to porous media consisting of homogeneous spheres with a single diameter D. The values of $K_{\text{H}_2\text{O}}$ for the stratified specimens can be calculated as the harmonic mean of the water permeabilities of the three homogeneous layers of equal thickness $h_i = 2$ cm, for $i = 1, 2, 3$:

$$K_{\text{H}_2\text{O}} = \frac{\sum_{i=1}^{3} h_i}{\sum_{i=1}^{3} \dfrac{h_i}{K_{\text{H}_2\text{O},i}}} = 1.25 \cdot 10^{-3}\ \text{m}\,\text{s}^{-1}. \tag{25}$$

All the empirical relationships return the hydraulic conductivity of a porous medium as a function of the porosity and of the viscosity of the fluid. We bare in mind that each

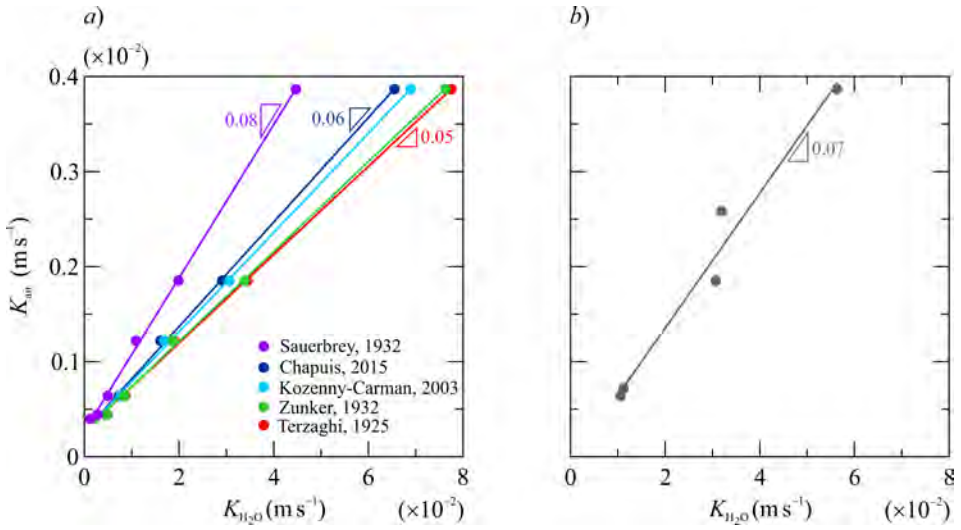

Figure 7: Experiments 1-7 with glass beads, 1-D permeameter. *a*) Measured air conductivity, K_{air}, plotted versus the hydraulic conductivity, $K_{\text{H}_2\text{O}}$, calculated through literature models for different kind of porous media; *b*) experimental air conductivity versus experimental water conductivity for specimens 3, 4, 5, 9, 10.

test #	d (mm)	K_{air} ($\times 10^{-3}$) (m s^{-1})	$K_{\text{H}_2\text{O}}$ ($\times 10^{-3}$) (m s^{-1})						
			Terzaghi (1925)	Sauebrej (1932)	Zunker (1932)	Kozeny-Carman (Carrier, 2003)	Chapuis (2015)	Mean	Std
1	0.5	0.40	1.82	1.24	2.12	1.92	1.82	1.77	0.29
2	0.75	0.44	4.09	2.79	4.77	4.31	4.09	3.89	0.72
3	1	0.64	7.28	4.96	8.47	7.66	7.28	6.80	1.42
4	2	1.85	29.11	19.86	33.89	30.64	29.11	26.30	7.17
5	3	3.87	65.49	44.68	76.25	68.95	65.49	58.26	17.90
6	1-2-3	1.22	16.04	10.94	18.67	16.89	16.04	14.79	3.43
7	3-2-1	1.16	16.04	10.94	18.67	16.89	16.04	14.79	3.43

Table 4: Comparison between the experimental air conductivity and the theoretical water conductivity. Porous medium of glass beads.

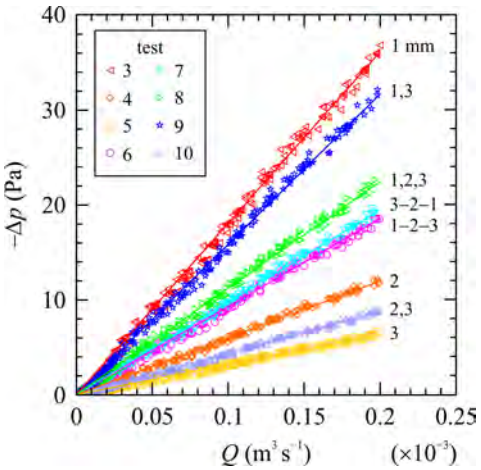

Figure 8: Glass beads specimens, differential pressure $-\Delta p$ as a function of the air flow rate Q in a 1-D flow geometry. The legend indicates the number of the tests that symbols refer to.

study refers to a medium with different properties (natural or artificial medium, with smooth or rough, rounded or irregular grains, etc.). This is the reason for the variability of the results which are shown in figure 7a, where the measured air conductivity is plotted versus the hydraulic conductivity calculated through literature models.

The numbers shown at the top of each straight line in figure 7a, represent the slope of the empirical models, with values in the range $0.05 - 0.13$, so $K_{\text{air}} = (0.05 - 0.13)\ K_{\text{H}_2\text{O}}$, or alternatively $K_{\text{H}_2\text{O}} = (7.7 - 20)\ K_{\text{air}}$, which is consistent with eq.(15), derived from dimensional analysis. Figure 7b shows the correlation between experimental air and water conductivity for some specimens of the present study. The slope 0.07 of the line lies in the theoretical range, and suggests that $r_K = 1/0.07 \approx 15$. This value of the scaling factor can be adopted to estimate the water conductivity of a porous medium (made of coarse glass beads) from the measured air conductivity.

Figure 8 shows the raw data of the differential pressure, $-\Delta p$, as a function of the flow rate, Q for the experiments $1 - 10$. The flow resistance increases for decreasing diameter as expected, with the mixtures and the stratified specimens presenting an intermediate response compared to their single components.

We can observe that:

- in the homogeneous samples, the conductivity increases with increasing glass beads diameter. As expected, with the growth of the particle dimension, also the void volume grows and the medium become more pervious;

- the difference in the conductivity of the stratified specimens ($1-2-3$ and $3-2-1$) is not significant, even though the conductivity in the fine-coarse direction, $K_{\text{air}} = 1.22 \cdot 10^{-3}\ \text{m s}^{-1}$, is 5% greater than in the coarse-fine direction, $K_{\text{air}} = 1.16 \cdot 10^{-3}\ \text{m s}^{-1}$, although the difference is well within the uncertainties. This was also found by [51] who associated this difference to an abrupt drop of the pressure at the interface between two media with different conductivity. This pressure drop induces an extra energy loss and reduced the overall conductivity of the stratified medium.

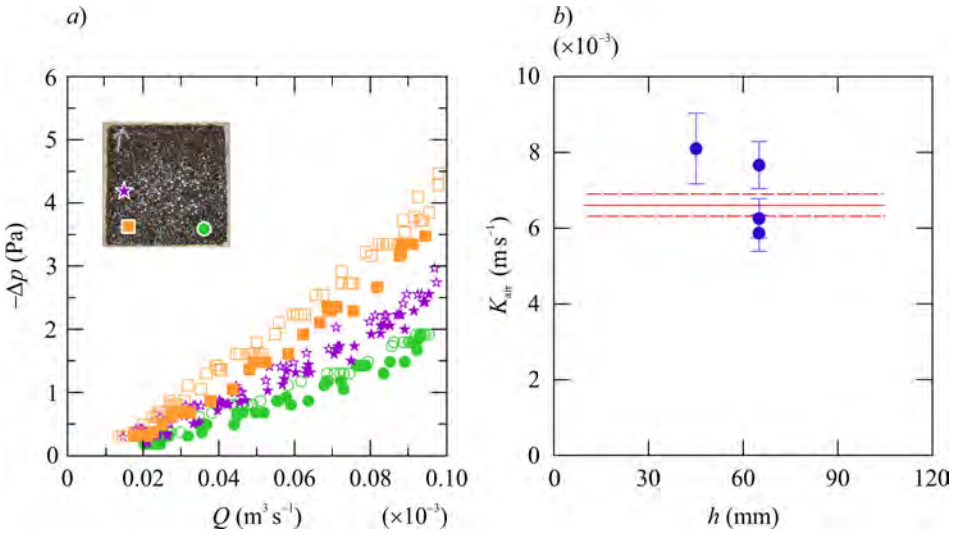

Figure 9: Asphalt samples, measurements on cores extracted from plates, 1-D flow configuration. *a*) Differential pressure $-\Delta p$ as a function of the air flow rate Q for cores from the same plate with thickness $h = 65$ mm; *b*) air conductivity K_{air} as a function of the thickness of the asphalt plate h. The solid red line represents the weighted average value, while the dotted red lines represent one weighted standard deviation.

However, we notice that this result is odd, since we expect larger dissipation, with a consequent reduced conductivity, for the expansion process of the flow in the fine-coarse direction;

- the value of the conductivity of the 2, 3 mixed specimen approximates the average of the conductivity of the single components. This is a consequence of an intermediate distribution of the voids between the 3 mm and 2 mm particles;
- the value of the conductivity of the 1, 3 mixed specimen is a little greater that the conductivity of the homogeneous specimen with 1 mm beads. A possible explanation is the greater difference between the 1 mm and 3 mm particles than the 2 mm and 3 mm particles. The empty spaces between the beads is more efficiently filled by the smallest particles, resulting in a slightly permeable medium.

5.2. 1-D hydraulic conductivity of asphalt samples

If we consider a heavy rainfall with intensity of 100 mm h^{-1}, and a circular cross-section with diameter of 100 mm, the water flux entering the sample results $Q_{\text{H2O,r}} = 0.22 \cdot 10^{-6}$ m^3 s^{-1}. The equivalent air flow rate is 10 times bigger, according to the dimensional analysis described in § 2, so $Q_{\text{air,r}} = 0.22 \cdot 10^{-5}$ m^3 s^{-1}. We remind you that the flow rate mainly depends on the flow of the adjacent pavement area, which can be much higher than the local influx, especially at the borders of the road.

The differential pressure $-\Delta p$ for the vertical conductivity of the cylindrical samples, shows a linear trend with the air flow rate Q, for $Q \leq 0.10 \cdot 10^{-3}$ m^3 s^{-1}, as it can be seen in figure 9a. This value is two order of magnitude greater than $Q_{\text{air,r}}$. This suggests

that, even during a rainfall such as the one described above, the flow through the asphalt pores of the pavement is laminar.

Figure 9a refers to three samples cored from the asphalt plate with thickness $h = 65$ mm. In the inset, the same symbols of the plots were used to indicate the region of the asphalt plate where the samples had been cored from. The measurements show some hysteresis, as the increasing (empty symbols) and decreasing (full symbols) branches do not superpose perfectly. In addition, the slope of straight fitting lines varies. This could be due to some damage caused by coring operations on small samples, since no hysteresis can be seen on the original asphalt plates, as discussed later, in § 5.3 .

Figure 9b shows the valued of the air conductivity of the three samples cored from the plate with thickness $h = 65$ mm and the value of one samples cored from the plate with thickness $h = 45$ mm.

The mean value for the air conductivity is evaluated as a weighted average, $\overline{K}_{\rm air}$, with a weighted standard deviation, σ_K, which are shown as a solid line and two dotted lines respectively in figure 9b, and calculated as follows:

$$\overline{K}_{\rm air} = \frac{\sum \frac{1}{\sigma_i^2} K_{{\rm air},i}}{\sum \frac{1}{\sigma_i^2}} = 6.6 \cdot 10^{-3}\ {\rm m\,s^{-1}}, \tag{26}$$

$$\sigma_K = \sqrt{\frac{1}{\sum \frac{1}{\sigma_i^2}}} = 0.3 \cdot 10^{-3}\ {\rm m\,s^{-1}}. \tag{27}$$

The extrapolated water conductivity is then $K_{\rm H_2O} \approx 10 K_{\rm air} \equiv (6.6 \pm 0.3) \cdot 10^{-2}\ {\rm m\,s^{-1}}$.

5.3. Tests on the asphalt plates

Figure 10a shows the differential pressure, $-\Delta p$, against the air flow rate, Q, measured by the field air permeameter, for five plates with increasing thickness. These data were collected prior to the drilling operations. In spite of the plate with $h = 65$ mm, the flow resistance increases for decreasing thickness, since the influence of the impervious condition at bottom of the plate may become relevant on the three dimensional structure of the flow.

Figure 10b shows the linear relationship between the pressure and the air flow rate for all the measuring points of the plates with different thickness, in the limit $Q < 0.20 \cdot 10^{-3}\ {\rm m^3\,s^{-1}}$.

The straight lines in figure 10a fit the data recorded for all the nine points of measurements for each asphalt plate, and the correlation coefficient is always greater then 0.95. We also evaluated the parameter a separately for each measurement point of the same plate, but there is not significant difference from the mean value. This indicates that there are not preferential flow paths due to the roll compaction of the sample, and the conductivity of the plate is uniform in space.

5.4. Evaluation of an equivalent dimensionless length scale for asphalt plates

In the case of the asphalt plates, we suggest that the main part of the flow can be described as the radial flow across an annulus with inner radius r_1, outer radius r_2, and

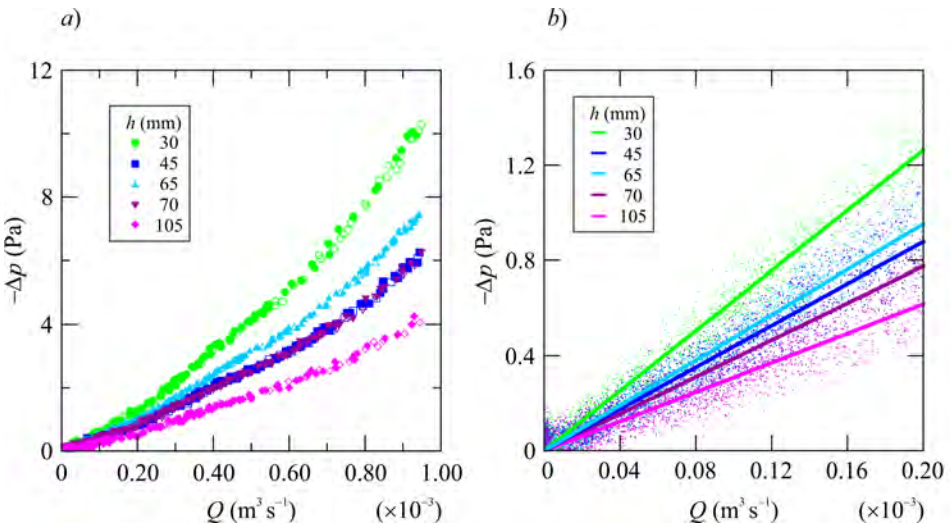

Figure 10: Asphalt plates, radial flux geometry. Differential pressure-discharge measurements for plates with different thickness. The measurements refer to the PMMA pipe positioned at the centre of the plate (point 5). (*a*) Whole set of data; (*b*) Data in the limit $Q < 0.20 \cdot 10^{-3}$ m^3 s^{-1}.

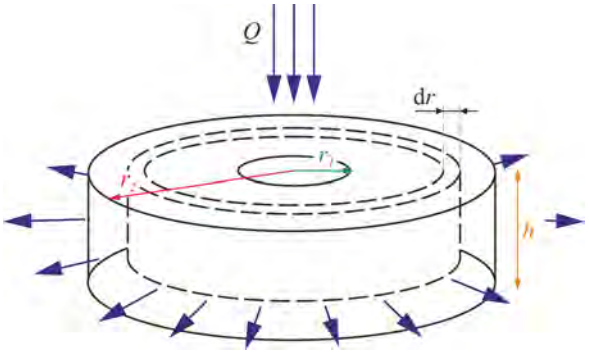

Figure 11: Schematic for the definition of the equivalent non dimensional length scale.

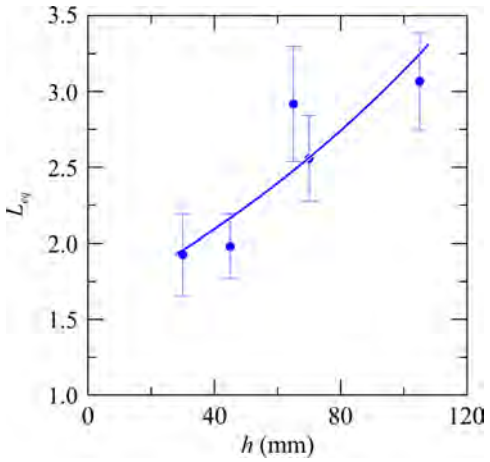

Figure 12: Equivalent non dimensional length scale L_{eq} as a function of the thickness h of the asphalt plates. Error bars are ± 1 standard deviation.

thickness h, as shown in figure 11. The Darcy formula for the annulus of thickness $\mathrm{d}r$ is

$$\mathrm{d}Q = \frac{K_{\mathrm{air}}\, 2\pi r h}{\gamma_{\mathrm{air}}} \frac{\mathrm{d}p}{\mathrm{d}r}, \tag{28}$$

where $2\pi r h$ is the lateral area of a cylinder with radius r, and $\mathrm{d}p/\mathrm{d}r$ is the pressure gradient. We can integrate eq.(28) by separation of the variables, obtaining:

$$L_{eq} \equiv \frac{r_2}{r_1} = \exp\left(\frac{K_{\mathrm{air}} 2\pi h a}{\gamma_{\mathrm{air}}}\right). \tag{29}$$

The ratio $L_{eq} = r_2/r_1$ is an equivalent non dimensional length scale relative to the asphalt plates. It can be evaluated as a function of the mean value of 1-D conductivity K_{air} measured on the cylindrical samples (eq. 26), on the thickness h and parameter a of the asphalt plate. Figure 12 shows the experimental L_{eq} as a function of h, for all the asphalt plates.

All the experimental data are consistent with the theoretical model within one standard deviation, with the exception of the asphalt plate with thickness $h = 65$ mm. The experimental equation that allows the computation of L_{eq} on the basis of the only thickness h, is:

$$L_{eq} = 1.6\, \exp(0.007\, h) \approx 1.6 + 0.11\, h, \qquad \text{for } 30 < h < 110 \text{ mm}, \tag{30}$$

with h expressed in mm ($R^2 = 0.80$). Inverting eq.(29) yields

$$K_{\mathrm{air}} \approx \frac{\gamma_{\mathrm{air}}}{2\pi h a} \ln(1.6 + 0.11h), \qquad \text{for } 30 < h < 110 \text{ mm}. \tag{31}$$

5.5. In situ experiments

A series of field tests were conducted to compare the value of r_K predicted by dimensional analysis (eq. 15) with field data. The available sites were (i) a service road inside

the Monza (Milan, Italy) racetrack and (ii) a urban road under construction in Poviglio (Reggio Emilia, Italy). The thickness of the porous asphalt pavement in Monza is $h = 70$ mm, while in Poviglio it is $h = 40$ mm. The parameters of the field tests are listed in tables 2−3.

Firstly, in both sites, we positioned the air field permeameter on the road axis, in the middle of the lanes, and close to the edges, at different cross-sections of the roads, and we measured the a parameter. The equivalent non dimensional length scale L_{eq} was estimated according to eq.(30) and the results show that $L_{eq} = 0.94$ in Monza and $L_{eq} = 0.74$ in Poviglio. The air conductivity can be estimated by reversing eq.(29):

$$K_{\text{air}} = \frac{\gamma_{\text{air}}}{2\pi h a} \ln (L_{eq}) \tag{32}$$

The mean values for the air conductivity are $K_{\text{air}} = (0.43 \pm 0.02) \cdot 10^{-3}\ \text{m}\,\text{s}^{-1}$ in Monza and $K_{\text{air}} = (1.00 \pm 0.08) \cdot 10^{-3}\ \text{m}\,\text{s}^{-1}$ in Poviglio.

Secondly, we measured the water conductivity by the falling head permeameter in some of the points where the K_{air} value was available. The mean values are $K_{\text{H}_2\text{O}} = (4.1 \pm 0.5) \cdot 10^{-3}\ \text{m}\,\text{s}^{-1}$ in Monza and $K_{\text{H}_2\text{O}} = (5.1 \pm 0.8) \cdot 10^{-3}\ \text{m}\,\text{s}^{-1}$ in Poviglio.

As a consequence the scale factors for the conductivity is $r_K = 9.6$ in Monza and $r_K = 5.1$ in Poviglio, which are of the same order of magnitude as predicted by the dimensional analysis, $r_K = \mathcal{O}(10)$.

We now shall compare our results with previous studies found in literature. Figure 13 gives an overview of the range of the hydraulic conductivity values of porous asphalt pavements, measured using falling head permeameters. The results by different authors are of the same order of magnitude and the differences can be addressed (i) to the different mix design of the asphalt mixtures and (ii) to the specific characteristics of the permeameter used by the authors.

As mentioned in § 1, [16] used two methods to test the water conductivity of porous asphalt pavements, the National Center for Asphalt Technology (NCAT) falling head permeameter and ASTM C1701 constant head permeameter. They found that the conductivity measured with the ASTM method lies in the range $K_{\text{H}_2\text{O}} = (0.6 - 1.1) \cdot 10^{-3}\ \text{m}\,\text{s}^{-1}$ and are 70% on average lower than the value measured with the NCAT method, which falls in the range $K_{\text{H}_2\text{O}} = (9.4 - 12) \cdot 10^{-3}\ \text{m}\,\text{s}^{-1}$.

On the other hand, [52] used the Laboratorio de Caminos de Santander (LCS) permeameter to measure the horizontal and vertical hydraulic conductivity on field plates as a function of the voids content. For voids content between $21 - 29\%$ the vertical conductivity grows from 3.2 to $9 \cdot 10^{-3}\ \text{m}\,\text{s}^{-1}$.

Lu *et al.* (2020) [53] investigated the conductivity of polyurethane-bound pervious materials, with effective porosity of approximately $28 - 29\%$, using a custom-made constant head permeameter developed according to the UNI EN 12697/19 protocol. They found that $K_{\text{H}_2\text{O}} = (3.4 - 5.3) \cdot 10^{-3}\ \text{m}\,\text{s}^{-1}$.

Each method has its advantages and disadvantages. This is principally why there are a lot of techniques and types of permeameters used by different authors in previous studies. For example, [16] discuss the implications of the results obtained by using the ASTM C1701 and NCAT permeameters. They say that the size of the permeameter ring may affect the results, as well as whether the measurements are made under constant head or falling head conditions. As it happens, ASTM C1701 gives higher values of permeability if operating under falling head than under constant head. Moreover, NCAT

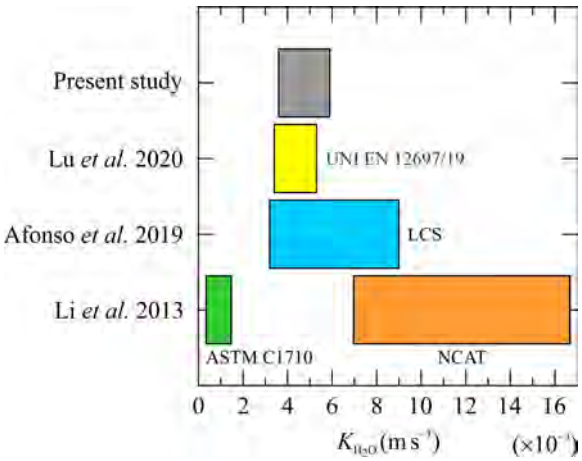

Figure 13: Comparison of values of the water conductivity $K_{\mathrm{H_2O}}$ from literature and present experiments.

method is more affected by errors in the knowledge of the thickness of the pavement than the ASTM, but at the same time, NCAT is based on a better established falling head theory derived by the Darcy's law, while the equation used in the ASTM method are not well explained. Similarly, [52] state that the results obtained with EN 12697-40 and EN 12697-19 are not directly comparable to each other and to other methods as well, such as the LCS.

Different ranges of the measured conductivity may arise because of misunderstanding of definitions and using of non-standard terminology between different authors, such as saturated hydraulic conductivity [20], infiltration capacity [6], permeability coefficient [54], or simply permeability [55, 24].

6. Conclusion

This paper presented a novel apparatus for measuring the in situ conductivity of porous asphalt pavements. This apparatus consists of a simple PMMA tube as air permeameter, a mass flow meter, a pressure gauge and a laptop for calibration and data acquisition. The positive sides of using air as fluid are that (i) a little time is necessary to establish pressure flow equilibrium, (ii) there is no need to carry a huge amount of fluid on site, as air is immediately available everywhere, (iii) the nature of the test is non destructive, as the crack size is not altered by the air flow, if applied for a short time.

The main conclusion are the followings.

- The 1-D permeameter was firstly calibrated using glass beads specimens. The ratio between the measured air and water conductivity is $r_K = 7.7$. This value is consistent with the value $r_K \approx 10$ suggested by dimensional analysis.
- Secondly, the air field permeameter was used in laboratory to estimate the parameter $a = -\Delta p/Q$ of asphalt plates with variable thickness. The vertical air conductivity of the asphalt plates was measured separately, using the Darcy formula, on cylindrical samples cored from each plate.

- We then derived a simple model for an estimate of an equivalent non dimensional length scale, L_{eq}, based on the knowledge of the only thickness of the porous asphalt plate. The value of L_{eq} could be used on site, together with the a parameter given by the air field permeameter, in order to compute the conductivity of the asphalt layer.

- Finally, some field tests were conducted on two available sites, in order to estimate the scale ratio r_K in field. The results are $r_K = 9.6$ in Monza and $r_K = 5.1$ in Poviglio, which are of the same order of magnitude as predicted by the dimensional analysis ($r_K = 10$).

We remind the readers that a variability of the results is expected, since the dimensional analysis followed by experiments captures the relevant dimensional groups that control the process, but cannot describe in detail the relationship between these groups. In particular the relationship r_K is site-specific and allows to control the time variation of the same pavement due, for example, to clogging phenomena and to plan maintenance. The instrument and methodology can be easily used to measure the effects of porous asphalt pavement drainage control systems in order to limit the disposal of de- and anti-icing solutions.

Future studies may focus on the changing of hydraulic permeability, and so the r_K parameter, because of crack propagation due to water damage or clogging phenomena. In this way the changing in r_K could be better related to a changing in the geometry of air voids. Also the effects of anisotropy of asphalt mixtures may be included in the theoretical model and measurement procedures, and the effects of surface tensions when water becomes in contact with pore edges.

Acknowledgements

This work was supported by the University of Parma - FIL incentivante 2019 - project: "Increased road safety on draining pavements through the development of percolation retardant fluids for anti-icing solutions."

List of symbols and acronyms

A	cross-section area of the pipe, L^2
A'	cross-section area of the sample, L^2
a	slope of the straight line fitting the experimental data $-\Delta p$ versus Q, $ML^{-4}T^{-1}$
ASTM	American Society for Testing and Materials
b	Klinkenberg slip coefficient, $ML^{-1}T^{-2}$
c	coefficient, (.)
$C_{KC,S,T,Z}$	constants, (.)
D	diameter, L
D_{int}	internal diameter, L
e	void ratio, (.)
Fr	Froude number, (.)
g	acceleration due to gravity, LT^{-2}

H	total head, L
h	thickness of asphalt plate, L
J	energy dissipation rate, (.)
K	conductivity, LT^{-1}
K_{air}	air conductivity, LT^{-1}
$K_{\text{H}_2\text{O}}$	water conductivity, LT^{-1}
Kn	Knudsen number, (.)
k	intrinsic permeability, L^2
k_∞	asymptotic intrinsic permeability, L^2
L	characteristic length path, L
l_1	initial level in the falling head permeameter, L
l_2	final level in the falling head permeameter, L
L_{eq}	equivalent length scale, L
l_m	mean free path of molecules, L
LCS	Laboratorio Caminos Santander permeameter
LPC	Leeds Permeability Cell
n	porosity, (.)
NCAT	National Center for Asphalt Technology falling head permeameter
p	pressure, $ML^{-1}T^{-2}$
Q	flow rate, L^3T^{-1}
r	radial coordinate, L
r_i	scale ratio for the quantity i, (.)
r_1	inner radius of the annulus, L
r_2	outer radius of the annulus, L
Re	Reynolds number, (.)
S_0	specific surface of particles, L^{-1}
u	velocity LT^{-1}
γ_{air}	air specific weight, $ML^{-2}T^{-2}$
γ_{H_20}	water specific weight, $ML^{-2}T^{-2}$
ΔH	head variation, L
Δp	differential pressure, $ML^{-1}T^{-2}$
Δt	time interval for the water column to flow though the sample, T
θ	temperature, Θ
κ	Boltzmann's constant, $ML^2T^{-2}\Theta^{-1}$
λ	length scale, L
μ	dynamic viscosity, $ML^{-1}T^{-1}$
ν_{air}	air kinematic viscosity, L^2T^{-1}
ν_{H_20}	water kinematic viscosity, L^2T^{-1}
ρ	density, ML^{-3}
σ_K	standard deviation of K, LT^{-1}
Φ	function

References

[1] G. Stotz, K. Krauth, The pollution of effluents from pervious pavements of an experimental highway section: first results, Science of the total environment 146 (1994) 465–70.

[2] C. Pagotto, M. Legret, P. Le Cloirec, Comparison of the hydraulic behaviour and the quality of highway runoff water according to the type of pavement, Water Research 34 (2000) 4446–54.
[3] J. Sansalone, X. Kuang, V. Ranieri, Permeable pavement as a hydraulic and filtration interface for urban drainage, Journal of irrigation and drainage engineering 134 (2008) 666–74.
[4] H. Imran, S. Akib, M. R. Karim, Permeable pavement and stormwater management systems: a review, Environmental technology 34 (2013) 2649–56.
[5] N. R. Siriwardene, A. Deletic, T. Fletcher, Clogging of stormwater gravel infiltration systems and filters: Insights from a laboratory study, Water research 41 (2007) 1433–40.
[6] V. C. Andres-Valeri, L. Juli-Gandara, D. Jato-Espino, J. Rodriguez-Hernandez, Characterization of the infiltration capacity of porous concrete pavements with low constant head permeability tests, Water 10 (2018) 480.
[7] Y. Ma, X. Chen, Y. Geng, X. Zhang, Effect of clogging on the permeability of porous asphalt pavement, Advances in Materials Science and Engineering 2020 (2020).
[8] M. Z. H. Mahmud, N. A. Hassan, M. R. Hainin, C. R. Ismail, R. P. Jaya, M. N. M. Warid, H. Yaacob, N. Mashros, Characterisation of microstructural and sound absorption properties of porous asphalt subjected to progressive clogging, Construction and Building Materials 283 (2021) 122654.
[9] D. M. Ramakrishna, T. Viraraghavan, Environmental impact of chemical deicers–a review, Water, Air, and Soil Pollution 166 (2005) 49–63.
[10] M. A. Cunningham, E. Snyder, D. Yonkin, M. Ross, T. Elsen, Accumulation of deicing salts in soils in an urban environment, Urban Ecosystems 11 (2008) 17–31.
[11] X. Shi, D. Veneziano, N. Xie, J. Gong, Use of chloride-based ice control products for sustainable winter maintenance: A balanced perspective, Cold Regions Science and Technology 86 (2013) 104–12.
[12] F. Autelitano, M. Rinaldi, F. Giuliani, Winter highway maintenance strategies: Are all the sodium chloride salts the same?, Construction and Building Materials 226 (2019) 945–52.
[13] UNI, Bituminous mixtures - Test methods for hot mix asphalt - Part 40: In situ drainability, Technical Report EN 12697-40:2006, 2006.
[14] ASTM International, Standard Test Method for Infiltration Rate of In Place Pervious Concrete, Technical Report ASTM Designation: C1701 / C1701M-09, 2009.
[15] ASTM International, Standard Test Method for Surface Infiltration Rate of Permeable Unit Pavement Systems, Technical Report ASTM Designation: C1781 / C1781M-18e1, 2018.
[16] H. Li, M. Kayhanian, J. T. Harvey, Comparative field permeability measurement of permeable pavements using ASTM C1701 and NCAT permeameter methods, Journal of Environmental Management 118 (2013) 144–52.
[17] L.-M. Chen, J.-W. Chen, T.-H. Chen, T. Lecher, P. C. Davidson, Measurement of permeability and comparison of pavements, Water 11 (2019) 444.
[18] MTC, Permeabilidad in sítu de pavimentos drenantes con el permeámetro LCS, Technical Report NLT 327/00, Ministerio de Transportes y Comunicaciones, 2000.
[19] M. T. Van Genuchten, A closed-form equation for predicting the hydraulic conductivity of unsaturated soils, Soil Science Society of America Journal 44 (1980) 892–8.
[20] P. Blackwell, A. Ringrose-Voase, N. Jayawardane, K. Olsson, D. McKenzie, W. Mason, The use of air-filled porosity and intrinsic permeability to air to characterize structure of macropore space and saturated hydraulic conductivity of clay soils, Journal of Soil Science 41 (1990) 215–28.
[21] B. V. Iversen, P. Moldrup, P. Schjønning, O. H. Jacobsen, Field application of a portable air permeameter to characterize spatial variability in air and water permeability, Vadose Zone Journal 2 (2003) 618–26.
[22] H. Li, J. J. Jiao, M. Luk, A falling-pressure method for measuring air permeability of asphalt in laboratory, Journal of Hydrology 286 (2004) 69–77.
[23] D. S. Springer, H. A. Loaiciga, S. J. Cullen, L. G. Everett, Air permeability of porous materials under controlled laboratory conditions, Ground Water 36 (1998) 558–65.
[24] T. Wells, S. Fityus, D. W. Smith, Use of in situ air flow measurements to study permeability in cracked clay soils, Journal of Geotechnical and Geoenvironmental Engineering 133 (2007) 1577–86.
[25] J. Cabrera, C. Lynsdale, A new gas permeameter for measuring the permeability of mortar and concrete, Magazine of Concrete Research 40 (1988) 177–82.
[26] J. Cabrera, T. Hassan, Quality control during construction of bituminous mixtures using a simple air permeability test, in: Performance and Durability of Bituminous Materials, Proceedings of Symposium, University of Leeds, 1996.
[27] S. E. Zoorob, J. G. Cabrera, L. B. Suparma, A gas permeability method for controlling quality of dense bituminous composites, Proc. 3rd European Symposium: Performance and Durability of

Bituminous Materials and Hydraulic Stabilised Composites (1999) 549–72.
[28] D. L. Allen, D. B. Schultz Jr, L. J. Fleckenstein, Development and proposed implementation of a field permeability test for asphalt concrete, Technical Report KTC-01-19/SPR216-001F, University of Kentucky, 2001.
[29] D. Perraton, A. Carter, In-situ permeability of the outermost layer of asphalt and cement concrete road materials: Water permeability evaluated with gas flow, Road Materials and Pavement Design 6 (2005) 239–53.
[30] P. Vardanega, State of the art: Permeability of asphalt concrete, Journal of Materials in Civil Engineering 26 (2012) 54–64.
[31] J. Chen, H. Wang, H. Zhu, Investigation of permeability of open graded asphalt mixture considering effects of anisotropy and two-dimensional flow, Construction and Building Materials 145 (2017) 318–25.
[32] E. Masad, A. Al Omari, H.-C. Chen, Computations of permeability tensor coefficients and anisotropy of asphalt concrete based on microstructure simulation of fluid flow, Computational Materials Science 40 (2007) 449–59.
[33] I. Gruber, I. Zinovik, L. Holzer, A. Flisch, L. D. Poulikakos, A computational study of the effect of structural anisotropy of porous asphalt on hydraulic conductivity, Construction and Building Materials 36 (2012) 66–77.
[34] V. Di Federico, R. Archetti, S. Longo, Similarity solutions for spreading of a two-dimensional non-Newtonian gravity current in a porous layer, Journal of Non-Newtonian Fluid Mechanics 177 (2012) 46–53.
[35] V. Di Federico, R. Archetti, S. Longo, Spreading of axisymmetric non-Newtonian power-law gravity currents in porous media, Journal of Non-Newtonian Fluid Mechanics 189 (2012) 31–9.
[36] V. Di Federico, S. Longo, S. King, L. Chiapponi, D. Petrolo, V. Ciriello, Gravity-driven flow of Herschel–Bulkley fluid in a fracture and in a 2D porous medium, Journal of Fluid Mechanics 821 (2017) 59–84.
[37] L. Chiapponi, V. Ciriello, S. Longo, V. Di Federico, Non-Newtonian backflow in an elastic fracture, Water Resources Research 55 (2019) 10144–58.
[38] B. S. Massey, Units, dimensional analysis and physical similarity, Van Nostrand Reinhold, 1971.
[39] S. Longo, Principles and Applications of Dimensional Analysis and Similarity, Springer International Publishing, 2021.
[40] L. Klinkenberg, The permeability of porous media to liquids and gases, in: Drilling and production practice, American Petroleum Institute, 1941.
[41] D. Faulkner, E. Rutter, Comparisons of water and argon permeability in natural clay-bearing fault gouge under high pressure at 20 °C, Journal of Geophysical Research: Solid Earth 105 (2000) 16415–26.
[42] Y.-S. Wu, K. Pruess, P. Persoff, Gas flow in porous media with Klinkenberg effects, Transport in Porous Media 32 (1998) 117–37.
[43] L. A. Cooley Jr, Permeability of Superpave mixtures: evaluation of field permeameters, Technical Report National Center for Asphalt Technology, NCAT Report, Auburn University, 1999.
[44] L. Chiapponi, Water retention curves of multicomponent mixtures of spherical particles, Powder Technology 320 (2017) 646–55.
[45] J. Říha, L. Petrula, M. Hala, Z. Alhasan, Assessment of empirical formulae for determining the hydraulic conductivity of glass beads, Journal of Hydrology and Hydromechanics 66 (2018) 337–47.
[46] K. Terzaghi, Principles of soil mechanics, Engineering News-Record 95 (1925) 19–32.
[47] F. Zunker, Zeitschrift fur pflanzenerwehrung (Fertilization and Soil Science), Duengung und Bodenkunde (Journal for Plant Nutrition) 25 (1932) 1.
[48] I. Sauerbrey, On the problem and determination of the permeability coefficient, Proceedings VNIIG (1932).
[49] W. D. Carrier III, Goodbye, Hazen; hello, Kozeny-Carman, Journal of Geotechnical and Geoenvironmental Engineering 129 (2003) 1054–6.
[50] R. P. Chapuis, S. Weber, F. Duhaime, Permeability test results with packed spheres and non-plastic soils, Geotechnical Testing Journal 38 (2015) 950–64.
[51] Z. Li, D. Wang, X. Zhang, J. W. Crawford, Water flow across the interface of contrasting materials: Pressure discontinuity and its implications, Journal of Hydrology 566 (2018) 435–40.
[52] M. I. L. Afonso, T. S. Santos, C. M. S. Fael, M. S. D. Almeida, Hydraulic conductivity of the permeable asphalt pavement–laboratory vs in situ test, in: IOP Conference Series: Materials Science and Engineering, volume 471, 2019, p. 022023.
[53] G. Lu, Z. Wang, P. Liu, D. Wang, M. Oeser, Investigation of the hydraulic properties of pervious

pavement mixtures: Characterization of darcy and non-darcy flow based on pore microstructures, Journal of Transportation Engineering, Part B: Pavements 146 (2020) 04020012.
[54] P. Bamforth, The relationship between permeability coefficients for concrete obtained using liquid and gas, Magazine of concrete research 39 (1987) 3–11.
[55] R. G. Shepherd, Correlations of permeability and grain size, Groundwater 27 (1989) 633–8.